Proceedings of the 21st ICSMGE, Vienna, Austria, 14 – 19 June 2026. Pistrol, Adam & Schweiger (eds.)
Published by: ÖGG, Austrian Society for Geomechanics, Salzburg, Austria, ISBN 978-3-9503898-4-5
https://doi.org/10.53243/ICSMGE2026-1834

Quantifying the actual evapotranspiration of a selected vegetation using a residual energy balance approach for landslide risk mitigation: a case study from the south-eastern Italian Apennine

Nico Stasi, Vito Tagarelli, Francesco Cafaro, Federica Cotecchia
Technical University of Bari, Italy, nico.stasi@poliba.it

ABSTRACT: The accurate quantification of evapotranspiration (ET) is critical for understanding the thermo-hydro-mechanical (THM) processes occurring within the topsoil stratum, where soil-vegetation-atmosphere (SVA) interface takes place, determining significant energy and hydraulic gradients. This study applies a residual energy balance (EB) method for soil cover surfaces to quantify ET flux over time, with reference to a case study of a clayey topsoil where selected vegetation, i.e., gramineous species, have been seeded and farmed since 2019. The case study is located in a pilot area, the South-eastern Italian Apennines, which is a region widely prone to landslide activity controlled by the SVA interaction. The method calculates actual ET (ET_a) as the residual term of the energy balance equation, utilizing net solar irradiance (Q*), sensible heat flux (H), and ground heat flux (G). The applied EB procedure was tested using monitoring data logged in the field, at the Pisciolo hillslope, by means of an on-purpose designed monitoring system setup. The computed values were compared with the reference crop calculated using the Penman–Monteith FAO 56 (ET_0). Results from the 2024 dataset show that ET_a was consistently different from ET (ET_0), with a seasonal divergence linked to vegetation phenology and soil moisture availability. The derived dynamic crop coefficient (Kc*) ranged from ~0.4 under summer water stress to >1.5 in early spring and late autumn.. Short-term analyses demonstrated rapid shifts from radiation-limited to moisture-enhanced ET following rainfall, while aerodynamic resistance and stability corrections confirmed the role of turbulence in controlling energy partitioning.

KEYWORDS : Nature-Based solution, evapotranspiration, energy balance method, landslide risk mitigation

1 INTRODUCTION

Evapotranspiration, ET, is a fundamental combination of processes within the soil–vegetation–atmosphere (SVA) interaction, influencing mass and energy transfers. Accurate quantification of ET is essential to assess the thermo-hydro-mechanical (THM) state of the rooted soil at the top of all geotechnical systems (Tagarelli and Cotecchia, 2025), i.e., the topsoil stratum, which is the most affected by the weather action and the vegetation state and behaviour (Moene et al., 2014).

In landslide-prone regions, such as the south-eastern Apennines in Italy, actual evapotranspiration, ET_a, influences the pore water pressure distribution and, thus, the slope stability (Cotecchia et al., 2019). Therefore, the quantification of ET_a is crucial for landslide risk assessment; at the same time, its measurement in situ provides insights into vegetation water uptake and soil water availability, in turn depending on the weather variable, on one side, and the hydro-mechanical behaviour of the rooted soils (Tagarelli et al., 2023 and 2024; Stasi 2024; Stasi et al., 2025).

The use of vegetation as a nature-based solution (NBS) for landslide risk mitigation should be based on a deep understanding of SVA interaction processes for the weather-plant-soil scenario of interest. Therefore, the measurement of ET_a in real, well-characterized field conditions is a key contribution to the development of NBS design.

The energy balance (EB) method represents a physically based approach to estimate ET_a by solving the surface energy balance (Anapalli et al., 2018). Although closure of the energy balance remains a challenge with the Eddy Covariance technique, EB models offer a viable alternative, especially in field crops using canopy-level measurements, and account for all relevant energy exchanges, also including latent heat flux (Anapalli et al., 2018). This method is suitable for application just above the plant canopy in the frictional sub-layer, the near-canopy zone directly influenced by roughness elements and extending roughly 0.2–0.5 times the canopy height above the vegetation. The EB approach applies the energy balance equation to a soil-vegetation system using a combination of near-surface soil sensors and atmospheric boundary layer sensors mounted on towers or remote platforms.

This study applies the EB approach to quantify ET_a with reference to a clayey slope in the south-eastern Apennines, where a gramineous vegetative cover has been established since 2019 (Tagarelli & Cotecchia, 2022; Stasi, 2024). The main objective is to validate the EB method using the monitoring data logged in the field and to compare ET_a with the reference evapotranspiration, ET_0, calculated via the FAO-56 Penman–Monteith equation (Allen et al., 1998). The derived crop coefficient (K_c*) can be, thereafter, used in hydrological modeling to support the prediction of run-off, and in geotechnical modelling, to predict the slope stability for any given crop condition, including vegetation used as NBS for landslide risk mitigation.

2 METHODOLOGY

2.1 *Energy balance approach to estimate ET_a*

The measurement of ET_a in this study is based on the application of the energy balance principle at the ground surface. In its general form, the energy balance is applied to a control volume that encompasses the vegetation canopy, the near-surface atmosphere, and the upper soil layers. The complete energy conservation equation for a control volume (Figure 1a) near the Earth's surface can be expressed as:

$$Q^* - \mathrm{H} - \mathrm{LvET} - \mathrm{G} + \mathrm{A}_h + \mathrm{A}_s = \Delta \mathrm{S}_{ha} + \Delta \mathrm{S}_{hv} + \Delta \mathrm{S}_{hs} + \Delta \mathrm{S}_{lat} \quad (1)$$

Where Q* is the net radiation, H is the sensible heat flux (energy contained in a substance that can be extracted by cooling it), LvET is the latent heat flux (latent heat can be extracted only by a phase change), G is the soil heat flux at the bottom boundary of the control volume, and A_h and A_s are the net advections contributions of sensible and latent heat, respectively. The right-hand side represents heat storage in the air, vegetation, and soil, and any change in latent energy within the volume if the inputs and outputs do not balance. All energy fluxes are expressed in $W \cdot m^{-2}$ and storage terms in $J \cdot m^{-2}$. Part of the solar radiation that hits the vegetation will be used for photosynthesis, but it is usually discarded.

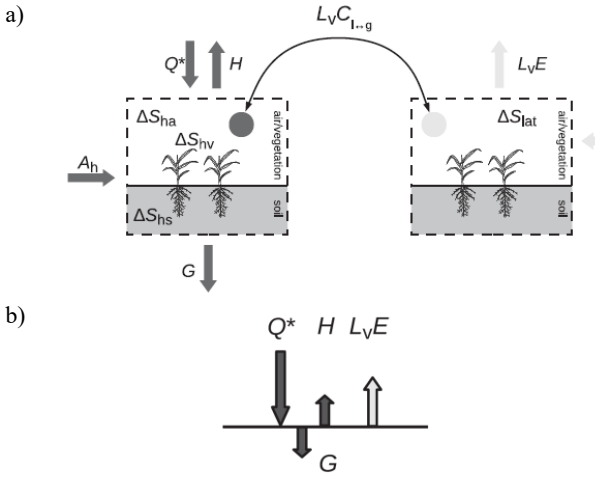

Figure 1. a) Control volume for energy balance: sensible heat (left, dark grey arrows) and latent heat (right, light grey arrows). Energy is exchanged between H and LvET if water changes phase (here, only phase changes between liquid and gas phase are considered: $LvC_{l\leftrightarrow g}$). Storage of energy in the form of chemical energy in the plants (due to assimilation), as well as some other terms, have been discarded. The direction of the arrows is for typical daytime conditions; b) Simplified surface water balance (Moene et al., 2014).

The latent heat flux transports energy through the transport of water vapour. The actual energy consumption related to evaporation is contained in the term $LvC_{l\leftrightarrow g}$ (Figure 1a), but because this term is internal to the control volume, it does not appear in the energy balance. The energy related to evaporation leaves the control volume as latent heat. In some cases, the latent heat flux leaving the control volume may not match the energy actually used for evaporation within the volume if there is either a change in water vapor storage (i.e., $\Delta S_{lat} \neq 0$) or non-zero horizontal advection of vapor. In this expression, all energy fluxes entering and leaving the volume are balanced against the temporal changes in energy storage within the volume. This framework captures the complete dynamics of energy exchange, including horizontal advection and internal storage.

Nevertheless, in surface-based energy balance models, such energies are typically neglected. Indeed, in practical field applications using the EB method, this volume-based formulation is simplified. The control volume is vertically compressed into an infinitesimally thin layer at the surface, i.e., control surface, which conceptually removes all volumetric storage and horizontal advection terms, as these are either negligible (ΔS_{soil}) or integrated into the surface flux measurements (Moene et al., 2014). In particular, the convective heat fluxes and latent heat fluxes (caused by ΔS_{hs}) in large pores are ignored because these are measured as sensible and latent heat flux in the atmosphere (Foken, 2008). This leads to the simplified energy balance equation widely used for ET estimation:

$$Q^* - G = LvET + H \quad (2)$$

In Equation 2, LvET is obtained as the residual term, once net radiation, ground heat flux, and sensible heat flux are measured or estimated independently. To compute evapotranspiration from Equation 2, the concept of resistance to turbulent exchange between the surface and the atmosphere (Foken, 2008) is employed. In this framework, the vegetation canopy is conceptualized as a "big leaf", and the energy exchange, specifically the latent heat associated with water vapour, is transported vertically through the atmospheric boundary layer against a turbulent resistance. The transfer of heat and vapor across the canopy–atmosphere interface also adheres to Fick's law, where the net flux is proportional to the gradient of concentration or temperature (Anapalli et al., 2018). This law enables the estimation of sensible and latent fluxes by combining vertical gradients with empirical models of aerodynamic resistance (r_a) through the turbulent boundary layer above the canopy.

2.2 *Description of energy components*

Net radiation (Q*) at the ground surface results from the balance between incoming shortwave solar radiation and longwave downwelling (heat) radiation from the atmosphere, minus the outgoing reflected shortwave and upwelling longwave radiation emitted by the surface. Only part of the incoming solar radiation is reflected; the rest is absorbed by the surface. The surface also absorbs longwave radiation emitted by clouds, particles, and atmospheric gases. This absorbed energy is partially emitted upward as longwave radiation. During daytime, the net radiation is typically positive, representing the total available energy that drives exchanges of heat and mass between the soil, vegetation, and atmosphere. Hence, in the total balance, the ground surface receives more radiation energy than is lost (i.e., Q* is positive). In contrast, the energy fluxes H and LvET and G are always energy fluxes towards the atmosphere or lower ground layers during the day, and in the opposite direction during the night. Only the latent heat flux is always a loss of energy for the ground surface except in the early morning hours with dewfall (i.e., when LvET is negative).

This energy surplus is partitioned into three major fluxes: sensible heat flux, which heats the overlying air; latent heat flux, which drives evapotranspiration; and ground heat flux, which transfers energy into the soil and is stored by the soil and plants. Sensible heat flux involves the turbulent transfer of energy from the surface to the atmosphere and is generally dominant during the day. It is responsible for heating the atmosphere from the surface up to some 100 m during the day, except for days with strong convection (Foken, 2008). Latent heat flux represents the energy used in the phase change of water and is directly proportional to the rate of evapotranspiration. Ground heat flux is primarily a conductive process that governs the energy exchange between the soil surface and deeper layers. For the generation of latent heat flux, an energy surplus at the ground surface is necessary, and water must be transported through the capillaries and pores of the soil. Energy for evaporation can also be provided by the soil heat flux in the upper soil layer. However, in the following, as already described, convective heat fluxes and latent heat fluxes in large pores are ignored, because these are measured as sensible and latent heat flux in the atmosphere.

The ground heat flux, G, is based mainly on molecular heat transfer and is proportional to the temperature gradient times the thermal molecular conductivity. In analogy to the molecular transport equations used for the calculation of the ground heat flux, the turbulent heat fluxes (sensible and latent) are often calculated using the vertical gradients of temperature T and specific humidity, respectively. However, the molecular transfer coefficients must be replaced by the turbulent diffusion coefficients. The sensible heat flux describes the turbulent transport of heat from and to the ground surface. The latent heat flux describes the vertical transport of water vapour and the heat required for evaporation at the ground surface.

Ground heat flux at the ground surface is typically estimated indirectly, as direct measurement near the soil surface is challenging due to steep thermal gradients in layers only a few

millimetres thick (Foken 2008) and uncertainties in topsoil thermal conductivity that change due to porosity, water content, and root presence (Moene et al, 2014). In practice, G is determined by combining the heat flux measured at depth using soil heat flux plates (generally called G_0) with the energy stored in the layer between the surface and the sensor. The uppermost millimeters of the soil often exhibit high thermal gradients during the day due to solar heating, while at night, the surface may cool more rapidly than the subsurface, leading to upward conduction.

Heat transfer in the atmosphere is much more effective than the molecular heat exchange in the soil, as it occurs through turbulent transport over a wide range of spatial and temporal scales of motions ranging from millimeters to kilometers (Foken, 2008). Turbulence facilitates the exchange of heat, water vapor, and even trace gases through eddy motion (The largest eddies are atmospheric pressure systems), which dominates over molecular conduction under most atmospheric conditions (Foken, 2008).

Sensible heat flux is commonly calculated based on the vertical temperature gradient between the canopy surface and the overlying air, modulated by aerodynamic resistance as:

$$H = \rho_a C_p (T_0 - T_a)/r_a \quad (3)$$

Where ρ_a is the density of air ($kg*m^{-3}$) calculated from the ideal gas equation, C_p is the specific heat of air assumed constant at 1005 J kg^{-1} K^{-1}, T_a is the air temperature at the sensor height (2 m) above the ground surface, and r_a is the bulk aerodynamic resistance to sensible heat transfer (sm^{-1}). The effective source temperature of sensible heat exchange is referred to as the aerodynamic temperature (T_0), which represents the level within the canopy where sensible heat is emitted. This temperature cannot be directly measured and is usually approximated by the surface temperature (T_s), which is obtained using a thermocouple placed beneath the canopy. In homogeneous canopies, the assumption $T_s \approx T_0$ is valid; however, in heterogeneous conditions, such an approximation may lead to substantial errors in the estimation of H (Chávez et al., 2005). Thus, T_0 reflects the interaction between soil properties and vegetation architecture. For computations of T_0 in this study, we used the equation developed empirically to estimate T_0 for different crop types (Chávez et al., 2005).

Latent heat flux (LvET) represents the energy consumed in the transformation of liquid water to vapor and is directly associated with the processes of soil evaporation, plant transpiration, and evaporation of intercepted water. This flux is tightly coupled to both the energy balance and the water balance, as evaporation requires both available moisture in the system and sufficient energy to sustain phase change. Consequently, evapotranspiration only occurs when both water and energy availability conditions are met.

A detailed mathematical formulation of the EB method can be found in Anapalli et al., 2018.

2.3 *Estimation of the Crop Coefficient (K_c*)*

As previously discussed, the main objectives of this work are to derive reliable Kc values over time for *Prati Armati®* gramineous vegetation and to develop a functional relationship between these Kc values and vegetation indices, such as leaf area index and root length density, across different growth stages (Stasi, 2024).

The FAO-56 model (Allen et al., 1998) is a widely adopted approach for estimating crop evapotranspiration (ET_c), wherein ET_c is calculated as the product of reference evapotranspiration (ET_0) and a crop coefficient (K_c, or the combination of $K_{cb} + K_e$ when adopting the dual coefficient approach; Allen et al., 1998). ET_0 reflects the evaporative demand of the atmosphere and corresponds to the evapotranspiration of a hypothetical reference crop (e.g., well-watered alfalfa crop), characterized by predefined properties such as height, albedo, and surface resistance. The reference evapotranspiration is estimated using the FAO-56 Penman–Monteith equation for a shorter time scale (i.e., every 15min) (Allen et al. 1998):

$$ET_0 = \frac{0.408\,\Delta\,(\mathrm{Rn} - \mathrm{G}) + \gamma \frac{37}{\mathrm{T}+273}\,\mathrm{u}_2\,(\mathrm{e_s} - \mathrm{e_a})}{\Delta + \gamma\,(1 + 0.34\,\mathrm{u}_2)} \quad (4)$$

Where Δ [kPa $^\circ$ C^{-1}] is the slope of the saturation vapor pressure curve, Rn is the net radiation at the crop surface, G is the soil heat flux density, (e_s–e_a) is the actual vapor pressure deficit, γ is the psychrometric constant, and u_2 is the wind speed measured at 2 m height.

By multiplying ET_0 by an appropriate crop coefficient K_c, which reflects the biophysical and physiological characteristics of the crop (e.g., canopy structure, ground cover, aerodynamic resistance), the model provides an estimate of potential crop evapotranspiration (ET_c).

In the single crop coefficient method, soil evaporation and crop transpiration are aggregated into a single K_c value, assigned to each crop growth stage. In contrast, the dual crop coefficient approach separates ET_c into two distinct components: transpiration (T_c), estimated using the basal crop coefficient (K_{cb}), and soil evaporation (E_s), calculated with the evaporation coefficient (K_e). Under ideal (i.e., non-limiting) conditions, consisting of inadequate water supply and optimal agronomic management, typical tabulated values of K_c or K_{cb} are used to estimate ET_c (Allen et al. 1998). However, in actual field scenarios, soil moisture limitations frequently induce water stress, thereby reducing evapotranspiration below its potential level. To account for this, the FAO-56 model incorporates a water stress coefficient (K_s), which ranges from 0 (severe stress) to 1 (no stress). Accordingly, actual crop evapotranspiration (ET_a) is typically lower than ET_c and can be described, under the single coefficient formulation, as:

$$ET_a = K_s \cdot K_c \cdot ET_o \quad (5)$$

The ratio between ET_a and T_0 over time represents the actual crop coefficient, K_c*, represented by the product between the standard unstressed crop coefficient, K_c, and the water stress coefficient, K_s. This formulation enables the estimation of real-time crop water use under varying soil moisture conditions, offering a dynamic and physically based interpretation of Kc that reflects both plant physiology and environmental stress.

2.4 *In-situ instrumentation*

The geotechnical characterization of the properties of the fine-grained topsoil of the structurally complex formations largely presents in the Southern Italian Apennines (Cotecchia et al., 2014), allowed to classify this material as silty clay with a slight sandy content, based on AGI (1994) classification. On average, its composition includes 45% clay fraction, 30% silt fraction, 21% sand fraction, and 4% gravel fraction. The specific gravity, liquid limit, and plastic limit were found to be 2.61, 68%, and 33%, respectively (Stasi et al., 2024).

The experimental setup design and installed in 2022 (Stasi, 2024) enables detailed tracking of the hydrological and thermal state of the slope system over time collecting data every 15min. The monitoring setup at Pisciolo hillslope involves a comprehensive and advanced network of sensors (> 40 sensors) installed along vertical profiles within the selected vegetation Prati Armati®, together with a weather station, which provides above-ground climatic data used in energy fluxes estimations

(Figure 2). All sensors are connected by wires to a datalogger (Campbell Scientific, Logan, UT, USA).

The EnviroSCAN™ sensors have been installed to measure the volumetric water content, VWC, in the soil using multiple sensors along an access tube embedded in the ground, providing VWC profiles to 2.5 m b.g.l. To allow for the monitoring of the net radiation, the SN-500 net radiometer has been chosen (Apogee Instruments, inc., Logan, USA). The whole net radiometer is made up of four different probes: two pyranometers and two pyrgeometers that are directed both upwards and downward. The sensors aimed at measuring the heat flux have been installed, which include a thermocouple (TCAV, Campell Scientific) and a heat flux plate (HFP01SC, Campell Scientific).

Figure 2. Monitoring setup in the Vegetate area (March 2024).

3 RESULT AND DISCUSSION

Monitoring the Pisciolo hillslope site began in May 2023; however, in this study, only data from the 2024 period are considered. All flux and meteorological measurements were processed and presented at a temporal resolution of 15 minutes, with evapotranspiration values expressed in millimeters per 15 minutes.

The climatic features of the area, located near Melfi in southern Italy, are largely controlled by altitude and Mediterranean mid-latitude conditions. The climate is characterized by marked seasonal fluctuations in both temperature and global radiation. Winters are generally cold and occasionally snowy, with average global radiation of ~40 W m^{-2} and mean air temperatures around 1 °C. Summers are hot and dry, with global radiation peaking around 680 W m^{-2} and maximum daily air temperatures reaching ~32 °C. Rainfall is distributed throughout the year, with the wettest period occurring from late autumn to early spring. Daily precipitation maxima rarely exceed 60 mm d^{-1} in winter. Relative humidity typically ranges between 60 and 95%, and wind speed between 0.1 and 10 m s^{-1}.

To analyze the result of the EB method, a two-day monitoring period is reported in Figure 3, showing different responses to atmospheric conditions and rainfall events. The EB over a vegetated surface revealed clear diurnal patterns in the surface energy balance components. Net radiation (Q*) exhibited a strong daily cycle, peaking around midday on both days, while the partitioning of energy into latent heat flux (LvET), sensible heat flux (H), and ground heat flux (G) reflected changes in cloud cover and rainfall.

On 24 May, a typical clear-sky day, net radiation peaked above 600 W m^{-2} at midday, driving substantial partitioning of available energy into both LvET and H. Latent heat flux dominated for most of the day, indicating active vegetation transpiration supported by VWC ranging between 0.05 and 0.32 m^3 m^{-3}. Interestingly, H rose sharply at midday to values comparable to LvET. The elevated sensible heat flux coinciding with the peak of Q* can be attributed to increased thermal gradients between the warmed surface and the overlying air, likely due to a dry, unstable boundary layer. This pattern indicates that not all available energy was converted into latent heat, possibly due to low soil water content (0.05 m^3 m^{-3} at 15cm depth) or temporary stomatal regulation. Ground heat flux followed the expected pattern, becoming positive during daytime (heat transfer into the soil) with a delayed peak relative to Q*, and negative at night (release of stored energy). These dynamics are consistent with Wilson et al., 2002 on vegetated surfaces, where latent heat dominates under well-watered conditions.

On 25 May, multiple rainfall events and increased cloud cover altered the EB dynamics. Net radiation was notably lower, with two smaller midday peaks (~300 W m^{-2}) likely due to intermittent cloudiness. A significant rainfall event (~7 mm) occurred in the early morning, followed by two lighter showers later in the day. These events induced rapid changes in surface energy partitioning, but only a light increase in water content at 15cm. Sensible heat flux became negative during the morning, indicating a cooling effect from rain and enhanced evaporative processes, consistent with observations in similar settings (Gao et al., 2004). Despite reduced Q*, latent heat flux remained active throughout the day, sustained by the increased soil water content from rainfall. The persistence of latent heat flux during the rainy day indicates a shift in partitioning toward evapotranspiration, as the wet soil surface and likely high stomatal conductance-maintained ET rates. This behavior aligns with Wilson et al. (2002), who reported that even moderate rainfall can sustain high ET when radiation remains sufficient.

These consecutive-day observations illustrate how, in mid-latitude climates, ET drivers can shift rapidly: on 24 May, ET was predominantly radiation-driven, while on 25 May, following rainfall, ET remained high despite lower radiation, suggesting that high soil VWC enhanced ET under sub-saturated atmospheric conditions (Teuling et al., 2010). This supports the framework that, while radiation generally dominates ET control on seasonal scales in humid temperate climates, short-term variability such as post-rain or drought events can shift the control toward soil moisture availability. The EB dynamics observed during these two days highlight the sensitivity of surface flux partitioning to both solar radiation and precipitation. The dominance of LvET over H, particularly under moist conditions, underscores the role of vegetation and soil water content in controlling energy exchanges in SVA interaction. In addition to the surface energy fluxes, the aerodynamic resistance (r_a) and the stability correction factor (ϕ) were analyzed to interpret the sensible heat flux behavior and the partitioning between latent and sensible heat. r_a was computed from the canopy–air temperature differential and wind speed, incorporating stability corrections for atmospheric conditions. On 24 May, r_a values remained relatively low (<100 s m^{-1}) for most of the day, consistent with unstable to near-neutral conditions and efficient turbulent transfer.

Conversely, during the night and early morning hours, r_a increased due to reduced mechanical turbulence and stable stratification, which limited sensible heat exchange. On 25 May, rainfall and increased cloud cover were associated with sharp fluctuations in r_a, with peaks exceeding 700–800 s m^{-1} during evening and night hours, indicating strong atmospheric stability and suppressed turbulent mixing. These high values correspond to periods when sensible heat flux approached zero or became negative, as surface cooling dominated. The stability

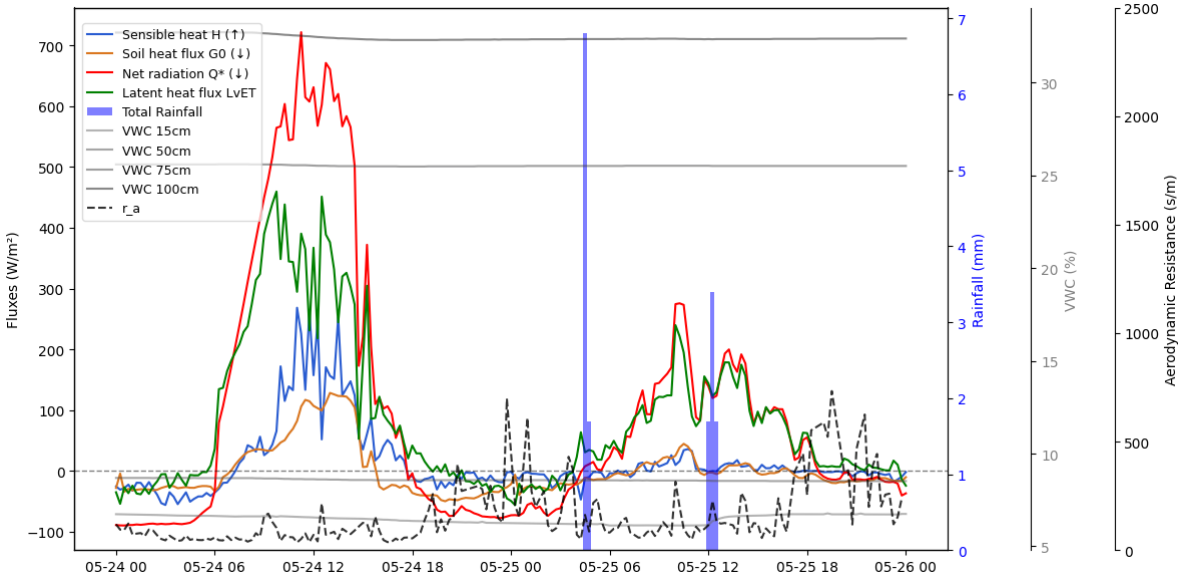

Figure 3. Diurnal patterns of energy fluxes, Aerodynamic resistance, rainfall and VWC on May 24, 2024 (non-rainy day) and on May 25, 2024 (rainy day) during the monitoring. Fluxes were computed and plotted in the graph at 15 m intervals.

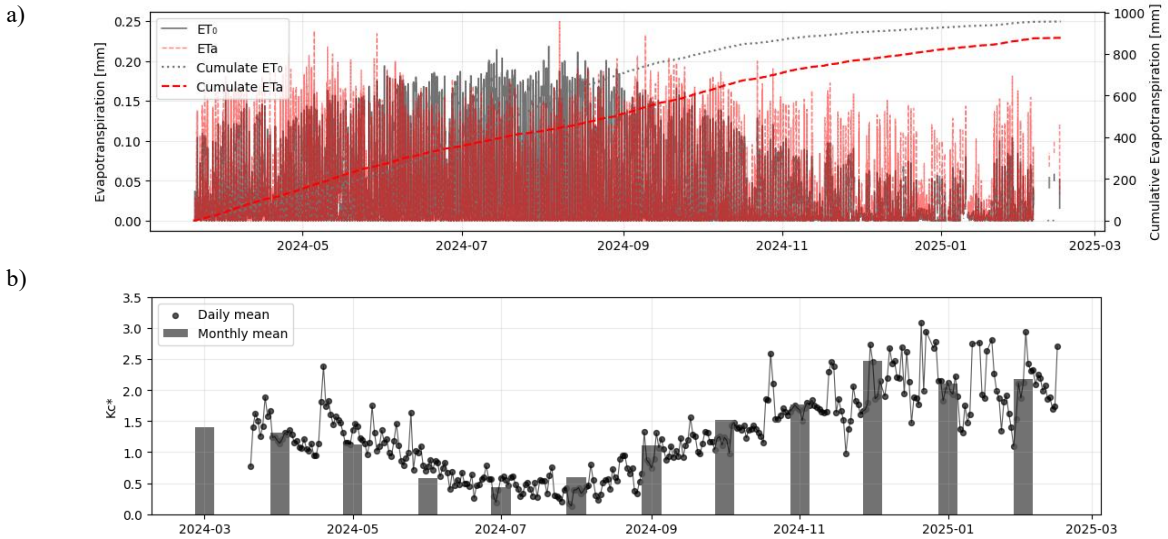

Figure 4. Actual evapotranspiration (ET_a) and FAO-56 reference evapotranspiration (ET_0) sub-daily values with their cumulative sums over the monitoring period; (b) daily and monthly mean values of the crop coefficient Kc*.

correction factor ϕ followed a similar pattern: values close to 1 during daytime unstable conditions, increasing markedly under stable nighttime conditions, and peaking during and after rainfall events on 25 May. This behavior aligns well with what was reported by Anapalli et al. (2018) for rainy days, where wet surfaces and reduced incoming radiation promoted stable atmospheric layers and lower turbulent exchange efficiency. The combined analysis of r_a and ϕ thus reinforces the interpretation of the flux partitioning patterns, linking the dominance of latent heat flux under wet conditions to both surface moisture availability and turbulence regime.

In Figure 4a, both actual evapotranspiration, ET_a, and FAO-56 reference evapotranspiration, ET_0, are shown, together with their cumulative sums over the monitoring period. Figure 4b reports daily and monthly mean values of the crop coefficient K_c*, computed as the ET_a/ET_0 ratio. ET_a consistently differs from ET_0, especially during summer, indicating that the selected vegetation's water use was reduced compared to a well-watered reference crop.

The cumulative ET values show a different trend. ET_a is higher in spring but then remains lower than ET_0 in summer. While reaching similar values in winter, Et_0 overestimates ET. K_c* displayed marked seasonal variation, from ~0.2 in the summer to peaks exceeding 2.5 in early spring and late autumn, suggesting higher canopy activity and transpiration efficiency during the active growth season.

The scatterplot in Figure 5 shows ET_a–ET_0 relationships by volumetric water content (VWC) class. At low VWC (0–5%, red), ET_a remained low regardless of ET_0. At intermediate VWC (5–30%, blue) and high VWC (30–50%, grey), ET_a scaled more linearly with ET_0, yet generally stayed above the 1:1 line, indicating reduced water stress and higher transpiration rates. This confirms an overall behaviour that is strongly controlled by the soil water content value, since the water stress condition has been seen to strongly suppress ET_a under dry

conditions, while wetter soils permit ET_a to approach and surpass the potential one. This pattern agrees with Doležal et al. 2018 and Anapalli et al. 2018, who applied an EB residual method to cotton and corn, finding close agreement with lysimeter ET measurements (RMSE ≈ 1.3 mm d^{-1} for cotton). Their study also demonstrated that EB methods incorporating variable aerodynamic resistance (r_a) and canopy temperature better capture real-time ET variability than when adopting the FAO-56 Penman-Monteith method, which implements fixed parameters. In FAO-56, ET_0 is standardized by assuming a constant surface resistance (r_s = 70 s m^{-1}) for reference grass (Allen et al., 1998). While this assumption simplifies comparisons, it can lead to hourly underprediction during periods of high radiation (when actual r_s is lower) and overprediction during low-radiation periods (when r_s is higher). Over daily time steps, such errors often compensate; however, in natural rainfed vegetation, r_s varies widely, especially under soil VWC deficit, causing ET_a to diverge from ET_0.

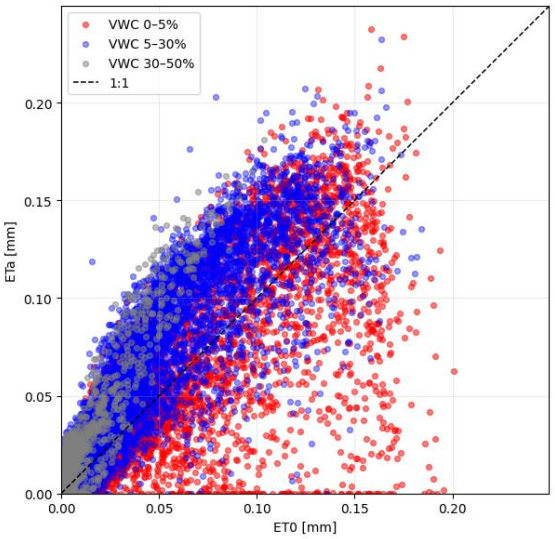

Figure 5. Sub-daily differences in Et_a and ET_0 for the monitored period classified by VWC.

4 CONCLUSION

This study applied the EB method to quantify ET_a over a selected vegetated hillslope in southern Italy, using 15-minute resolution micrometeorological and soil parameter measurements. The results demonstrated a clear seasonal divergence between ET_a and ET_0. The derived dynamic crop coefficient (K_c*) exhibited strong temporal variability, highlighting the combined influence of vegetation phenology and VWC on canopy water use. In particular, the correlation between ET_a/ET_0 and soil moisture content (VWC) highlights the critical role of water availability in modulating actual evapotranspiration. This improves crop-coefficient accuracy and, in the long term, supports the design of effective NBS for landslide mitigation. Since vegetation controls infiltration and evapotranspiration, an accurate estimation of ET_a is essential for predicting deep piezometric heads and ensuring slope stability.

5 AKNOWLEDGEDGEMENTS

This research was funded by project MITIGO, ARS01_00964, and project PNRR, MISURA M4_C2_1.4, (CN_00000013 CUP: D93C22000430001)—Spoke 5 “Environment and Natural Disasters”.

6 REFERENCES

Allen, R.G., Pereira, L.S., Raes, D. & Smith, M. 1998. *Crop evapotranspiration – Guidelines for computing crop water requirements*. FAO Irrigation and Drainage Paper No. 56. Rome.

Anapalli, S.S., Green, T.R., Reddy, K.N., Gowda, P.H., Sui, R., Fisher, D.K., ... & Marek, G.W. 2018. Application of an energy balance method for estimating evapotranspiration in cropping systems. *Agricultural Water Management*, 204, 107–117.

Chávez, J.L., Howell, T.A., Gowda, P.H., Copeland, K.S. & Prueger, J.H. 2010. Surface aerodynamic temperature modeling over rainfed cotton. *Transactions of the ASABE*, 53(3), 759–767.

Cotecchia, F., Tagarelli, V., Pedone, G., Ruggieri, G., Guglielmi, S. & Santaloia, F. 2019. Analysis of climate-driven processes in clayey slopes for the early-warning system design. *Proceedings of the Institution of Civil Engineers,*172, 463–4641.

Doležal, F., Hernandez-Gomis, R., Matula, S., Gulamov, M., Miháliková, M. & Khodjaev, S. 2018. Actual evapotranspiration of unirrigated grass in a smart field lysimeter. *Vadose Zone Journal*, 17(1), 1–13.

Foken, T., & Mauder, M. 2008. *Micrometeorology* (Vol. 2, p. 306). Berlin: Springer.

Gao, W., Shaw, R.H. & Paw U, K.T. 2004. Observation and modeling of the thermal effects of rainfall on the soil–plant–atmosphere system. *Agricultural and Forest Meteorology*, 122(1–2), 33–43.

Glade, T. 2003. Landslide occurrence as a response to land use change: A review of evidence from New Zealand. *Catena*, 51(3–4), 297–314. doi:10.1016/S0341-8162(02)00170-4.

Moene, A.F. & Van Dam, J.C. (2014) *Transport in the atmosphere–vegetation–soil continuum*. Cambridge University Press.

Stasi, N. 2024. Experimental and numerical study of Soil–Vegetation–Atmosphere interaction for the design of Nature-Based Solutions in landslide risk mitigation. PhD thesis, University of Bari.

Stasi N., Tagarelli V., Cafaro F. Cotecchia F., 2024. On the wildfire-induced changes in the properties of a vegetated clayey slope cover. *Proceedings of the 7th ISC7 Barcelona*, 18 - 21 June 2024.

Stasi, N., Tagarelli, V., Cafaro, F. 2024. The impact of a wildfire on a vegetated topsoil: field monitoring and numerical modelling. *CUTE, Poland, Wrocław,* 14-17 October 2024.

Stasi N., Tagarelli V., Cafaro F. Cotecchia F., 2024. On the Use of a Water Potential Probe for Suction and Temperature Measurements in Unsaturated Natural Clayey Soil. *Applied Sciences 15.6 (2025): 3021.*

Stasi, N., Tagarelli, V., Cafaro, F., Cotecchia, F. 2025. Thermo-hydro-mechanical field monitoring of a clayey topsoil: insights of the soil-vegetation-atmosphere interaction. *9th ISGSR. Oslo, Norway.*

Stasi, N., Tagarelli, V., Cafaro, F., Cotecchia, F. 2025. Field Monitoring of Soil–Vegetation–Atmosphere Interaction in a Clayey Hillslope for Nature-Based Landslide Mitigation. *Proceedings of RootS25, Bari.*

Tagarelli, V. & Cotecchia, F. 2022. Preliminary field data of selected deep-rooted vegetation effects on the slope–vegetation–atmosphere interaction: Results from an in-situ test. *Rivista Italiana di Geotecnica*, 56(1), 62–83.

Tagarelli, V. & Cotecchia, F. 2025. Weather-induced landslide activity in clayey slopes: Modeling for the design of site-scale early warning systems. *Journal of Geotechnical and Geoenvironmental Engineering*, 151(9), 04025092.

Tagarelli, V., Cotecchia, F., Stasi, N. & Cafaro, F. 2024. Root-induced changes in the hydraulic properties of a fine slope cover. *E3S Web of Conferences*, 544, 16002.

Tagarelli, V., Cotecchia, F. & Stasi, N. 2023. Numerical back-analysis of in-situ constant head tests in partially saturated soil cover to determine the permeability function. In *Proceedings of the National Conference of the Researchers of Geotechnical Engineering*, Palermo, Italy, 5–7 July 2023.

Teuling, A.J., Hirschi, M., Ohmura, A., Wild, M., Reichstein, M., Ciais, P., et al. 2010. Contrasting response of European forest and grassland energy exchange to heatwaves. *Nature Geoscience*, 3(10), 722–727.

Wilson, K., Goldstein, A., Falge, E., Aubinet, M., Baldocchi, D., Berbigier, P., et al. 2002. Energy balance closure at FLUXNET sites. *Agricultural and Forest Meteorology*, 113(1–4), 223–243.